Inhibition of miR-199a-3p Enhances Neuronal Differentiation of Bone Marrow Mesenchymal Stem Cells and Promotes Functional Recovery Following Spinal Cord Injury

Defeng ZOU[1], Weijian REN[1], Tingyu LIU[2], Jun LIU[1], Guanpeng XU[1], Shubo ZHANG[1], Xiaojiu LI[3], Wanshu GUO[3]

[1]Fifth Department of Orthopedics, Liaoning Provincial People's Hospital, Shenyang, Liaoning, China, [2]West China Medical School, Sichuan University, Chengdu, Sichuan, China, [3]Department of Neurology, Liaoning Provincial People's Hospital, Shenyang, Liaoning, China

Received February 27, 2026
Accepted July 21, 2026

Summary

Bone marrow mesenchymal stem cells (BMSCs) hold considerable promise for neural repair following spinal cord injury (SCI); however, their limited neuronal differentiation capacity remains a major translational barrier. MicroRNAs are critical regulators of stem cell fate, yet the specific miRNAs that constrain the neurogenic potential of BMSCs and the mechanisms through which they act remain incompletely defined. Comparative miRNA profiling of BMSCs, cortical neurons, and neural stem cells was performed using GeneChip microarray. The most differentially expressed miRNA, miR-199a-3p, was inhibited in BMSCs using a lentiviral sponge construct. Neuronal-like differentiation was evaluated by immunofluorescence and Western blot for β-III tubulin, MAP-2, and mTOR. Therapeutic efficacy was assessed in a rat T10-T11 contusion SCI model (n=20 per group) using the Basso-Beattie-Bresnahan (BBB) locomotor scale over 42 days. miR-199a-3p was the most significantly upregulated miRNA in BMSCs relative to neural cell populations. Sponge-mediated inhibition significantly reduced miR-199a-3p expression ($p<0.01$) and elevated mTOR protein levels. Anti-miR-199a-3p BMSCs expressed the neuronal markers β-III tubulin and MAP-2 and adopted neurite-like morphological features *in vitro*. In the SCI model, transplantation of anti-miR-199a-3p BMSCs yielded significantly greater locomotor recovery (BBB score: 15.7±0.6) compared with empty vector-transduced BMSCs (13.0±0.8) and vehicle control groups (10.8±0.6) at six weeks post-injury ($p<0.05$). Selective inhibition of miR-199a-3p enhances the neurogenic potential of BMSCs, in part by derepressing mTOR, and significantly improves functional outcomes following SCI transplantation.

Key words

miR-199a-3p • Bone marrow mesenchymal stem cells • Neuronal differentiation • mTOR • Spinal cord injury

Corresponding author

W. Guo, Department of Neurology, Liaoning Provincial People's Hospital, No. 33 Wenyi Road, Shenhe District, Shenyang, Liaoning 110016, China. E-mail: guowanshu1@126.com

Introduction

Spinal cord injury (SCI) represents a significant clinical challenge, often resulting in permanent loss of motor function, sensation, and autonomic control below the level of injury [1]. Cell-based therapeutic strategies aimed at replacing lost neural tissue have emerged as a promising avenue for SCI treatment [2]. Neural stem cell transplantation has attracted considerable research interest; however, the primary sources of neural stem cells are embryonic tissues, which raises substantial ethical and legal concerns that limit their clinical application [3].

Bone marrow-derived mesenchymal stem cells (BMSCs) offer an attractive alternative cell source for regenerative medicine applications. BMSCs possess several advantageous properties, including abundant availability, ease of autologous harvest, compatibility with autologous transplantation without risk of immune rejection, and freedom from ethical constraints [4,5]. Under appropriate conditions, BMSCs can be induced to differentiate into multiple cell lineages *in vitro*, including osteoblasts,

 An open access article under the CC BY 4.0 license https://creativecommons.org/licenses/by/4.0/ © 2026 by the authors. Published by the Institute of Physiology, Czech Academy of Sciences, Prague, Czech Republic. E-mail: physres@fgu.cas.cz, www.biomed.cas.cz/physiolres

myofibroblasts, chondrocytes, adipocytes, and cells exhibiting neural phenotypes [6]. Furthermore, cultured BMSCs demonstrate low immunogenicity and exhibit homing capacity to sites of injury, characteristics that enhance their potential for clinical translation [7]. Despite these favorable attributes, the molecular mechanisms governing BMSC differentiation toward neural lineages remain incompletely understood, and strategies to enhance the efficiency of directed neuronal differentiation represent an important area of ongoing investigation.

MicroRNAs (miRNAs) are endogenous, evolutionarily conserved small RNA molecules of 20-24 nucleotides that regulate gene expression post-transcriptionally. These molecules exert their regulatory effects by binding to complementary sequences within the 3′-untranslated regions (3′-UTR) of target messenger RNAs, thereby inhibiting translation or promoting mRNA degradation [8]. Accumulating evidence indicates that miRNAs play essential roles in neural development and neuronal function [9]. For instance, the brain-enriched miRNAs miR-9/9* and miR-124 facilitate the assembly of neuron-specific ATP-dependent chromatin remodeling complexes (BAF) and can direct the conversion of human dermal fibroblasts toward post-mitotic neuronal fates [10]. These findings suggest that manipulation of specific miRNAs may provide a means to enhance neuronal differentiation of stem cell populations.

Although a small number of miRNAs (e.g., miR-124, miR-9/9*) have been characterized as pro-neurogenic in fibroblast and neural progenitor systems, the miRNAs that actively constrain the acquisition of a neuronal phenotype in BMSCs have not been systematically identified. Such miRNAs could therefore serve as targets for enhancing BMSC-based neural repair. To address this gap, we performed comparative miRNA expression profiling of BMSCs, cortical neurons, and neural stem cells using microarray analysis. This screen identified miR-199a-3p as the miRNA showing the largest positive differential expression in BMSCs relative to both neural cell populations. miR-199a-3p was prioritized for functional interrogation for two reasons: (i) it exhibited the greatest fold-change of any candidate identified in the screen, and (ii) it has been shown in independent contexts to directly target the mammalian target of rapamycin (mTOR) by binding to its 3′-UTR, thereby suppressing mTOR protein expression [11,12]. Because mTOR signaling promotes axonal growth and neural regeneration [13,14], miR-199a-3p represented a candidate whose selective inhibition might simultaneously enhance a growth-permissive intracellular program in BMSCs.

Based on these considerations, we tested the central hypothesis that elevated miR-199a-3p expression represents a molecular barrier to the neurogenic differentiation of BMSCs through suppression of mTOR, and that selective inhibition of miR-199a-3p would enhance neuronal marker acquisition *in vitro* and improve functional recovery following BMSC transplantation in a rat model of spinal cord injury. The specific objectives of the present study were: (i) to identify miRNAs differentially expressed between BMSCs and neural cell populations; (ii) to determine whether sponge-mediated inhibition of miR-199a-3p enhances neuronal-like differentiation and derepresses mTOR expression in BMSCs; and (iii) to evaluate the therapeutic efficacy of anti-miR-199a-3p BMSCs in a rat contusion SCI model.

Materials and Methods

Cell acquisition, culture, and characterization

Sprague-Dawley (SD) rat neural stem cells, embryonic day 18.5 SD rat cortical neurons, and SD rat bone marrow mesenchymal stem cells (BMSCs) were obtained from Cyagen Biosciences Inc. (Guangzhou, China). Cell identity was verified by the supplier through flow cytometric analysis of surface markers ($CD29^+$, $CD44^+$, $CD45^-$, $CD34^-$ for BMSCs; Nestin+ for neural stem cells) and morphological assessment prior to shipment. Cortical neurons were cultured on poly-D-lysine-coated plates at a density of 1×10^6 cells/ml in Dulbecco's Modified Eagle Medium (DMEM; Gibco, Grand Island, NY, USA) supplemented with 10 % fetal bovine serum (FBS; Gibco). Following an initial attachment period of 4-6 h, the culture medium was replaced with Neurobasal medium (Gibco) supplemented with 2 % B27, 100 U/ml penicillin, 100 μg/ml streptomycin, and 0.5 mM glutamine (Gibco). All cultures were maintained in a humidified incubator at 37 °C with 5 % CO_2, and the medium was replenished every three days. BMSCs were used between passages 3 and 5 for all experiments to ensure consistent cellular characteristics.

MicroRNA expression profiling by GeneChip microarray

Total RNA, including the small RNA fraction, was extracted from BMSCs, neural stem cells, and cortical neurons using the miRNeasy kit (Qiagen, Frankfurt, Germany) according to the manufacturer's protocol. RNA integrity was assessed using an Agilent

2100 Bioanalyzer (Agilent Technologies, Santa Clara, CA, USA), and only samples with RNA integrity number (RIN) values greater than 8.0 were used for subsequent analysis. RNA concentration and purity were determined spectrophotometrically by measuring absorbance at 260 and 280 nm. Three independent biological replicates were prepared for each cell type. Microarray hybridization and analysis were performed by Affymetrix (Santa Clara, CA, USA) using their GeneChip miRNA Array platform. Differential expression was defined as a fold change greater than 2.0 with an adjusted p-value <0.05 following Benjamini-Hochberg correction for multiple comparisons.

Quantitative Real-Time Reverse Transcription Polymerase Chain Reaction (qRT-PCR)

Total RNA was isolated using TRIzol reagent (Invitrogen, Guangzhou, China) according to the manufacturer's instructions. Complementary DNA (cDNA) was synthesized using reverse transcriptase (Life Technologies, Carlsbad, CA, USA) following the protocol provided by Fermentas Corporation. Quantitative PCR was performed on an ABI 7500 Real-Time PCR System (Applied Biosystems, Foster City, CA, USA) using SYBR Green I detection chemistry (TOYOBO, Osaka, Japan). The thermal cycling parameters consisted of an initial denaturation at 95 °C for 3 min, followed by 40 cycles of 95 °C for 20 s and 60 °C for 30 s, with a final melting curve analysis at 95 °C for 10 s. U6 small nuclear RNA served as the endogenous reference for normalization of miRNA expression levels. All reactions were performed in triplicate, and relative expression was calculated using the $2^{-\Delta\Delta Ct}$ method. No-template controls were included in each run to monitor for contamination.

Construction of miR-199a-3p-sponge lentiviral vector

The lentiviral vector pLVX-EN-rno-miR-199a-3p-sponge was designed and constructed by Yingrun Biotechnologies Inc. (Changsha, China). The sponge sequence, containing multiple tandem binding sites complementary to miR-199a-3p with a central bulge region of approximately four base pairs, was cloned into the pLVX-EGFP-IRES-neo backbone. The bulge design enables miRNA sequestration while preventing Argonaute-mediated cleavage of the sponge transcript. For lentivirus production, 293FT packaging cells were transiently co-transfected with pLVX-EN-rno-miR-199a-3p-sponge (10 μg), pLP1 (6.5 μg), pLP/VSVG (3.5 μg), and pLP2 (2.5 μg) using Lipofectamine 2000 Reagent (Invitrogen, Carlsbad, CA, USA). The 293FT cells were cultured in DMEM supplemented with 10 % FBS and were seeded at 80 % confluence 24 h prior to transfection. Viral supernatants were harvested 48 and 72 h post-transfection, filtered through 0.45-μm membranes, and concentrated by ultracentrifugation. The empty vector pLVX-EN-rno served as the negative control. Viral titer was determined by serial dilution and quantification of GFP-positive cells using fluorescence microscopy. Successful vector construction was confirmed through restriction enzyme digestion with XhoI and BamHI, followed by DNA agarose gel electrophoresis, and was further validated by Sanger sequencing at Yingrun Biotechnologies Inc.

Lentiviral transduction of BMSCs and differentiation conditions

BMSCs were seeded in six-well plates at a density of 2×10^5 cells per well and allowed to adhere for 24 h prior to transduction. Cells were divided into three experimental groups: (1) control group (untransduced BMSCs), (2) empty vector group (BMSCs transduced with the empty vector pLVX-EN-rno), and (3) anti-miR-199a-3p group (BMSCs transduced with pLVX-EN-rno-miR-199a-3p-sponge). Transduction was performed at a multiplicity of infection (MOI) of 10 in the presence of 8 μg/ml polybrene (Sigma-Aldrich, St. Louis, MO, USA) to enhance transduction efficiency. The medium was replaced with fresh culture medium 24 h post-transduction. Transduction efficiency was assessed by visualization of GFP expression under fluorescence microscopy at 72 h post-transduction. Only cell populations exhibiting greater than 80 % GFP positivity were used for subsequent experiments.

Following transduction, BMSCs from all three groups were maintained under standard growth conditions (DMEM supplemented with 10 % FBS, penicillin/streptomycin, and glutamine) without the addition of exogenous neurogenic supplements (such as retinoic acid, β-mercaptoethanol, forskolin, dbcAMP, or defined neural induction media). This design was chosen to determine whether inhibition of miR-199a-3p was sufficient on its own to promote acquisition of neuronal markers and neurite-like morphology in the absence of external neurogenic cues. Cells were assessed for neuronal marker expression and morphology after six days of *in vitro* culture under these standard conditions.

Immunofluorescence detection of neuronal markers

Following six days of *in vitro* culture post-transduction, cells from all three experimental groups were fixed with 4 % paraformaldehyde for 15 min at room temperature, then rinsed three times with phosphate-buffered saline (PBS; 10 min per wash). Non-specific binding was blocked by incubation with 10 % normal goat serum for one hour at room temperature. Cells were then incubated overnight at 4 °C with the following primary antibodies: mouse anti-β-III tubulin (1:100 dilution) and mouse anti-MAP-2 (1:50 dilution). Primary antibody specificity was confirmed using appropriate isotype controls. Following three PBS washes (10 min each), cells were incubated with secondary antibodies, including DyLight 488-conjugated goat anti-mouse IgG (green fluorescence) and Texas Red-conjugated rabbit anti-mouse IgY, for one hour at 37 °C in the dark. After final PBS washes (three times, 5 min each), nuclei were counterstained with 4′,6-diamidino-2-phenylindole (DAPI; 1:1000) for 10 min at room temperature. Immunofluorescence images were acquired using a fluorescence microscope (Model 2013) at 200× magnification. Images were captured from at least five random fields per experimental condition, and experiments were performed in triplicate.

Western blot analysis

Cells were harvested and lysed on ice with PMSF-containing lysis buffer (Applygen Technologies Inc., Beijing, China) for 30 min. Lysates were clarified by centrifugation at 12,000× g for 5 min at 4 °C, and total protein concentration was quantified using the bicinchoninic acid (BCA) protein assay kit (ShineGene, Shanghai, China). Equal amounts of protein (50 μg per lane) were separated by sodium dodecyl sulfate-polyacrylamide gel electrophoresis (SDS-PAGE) on 5-10 % gradient gels and subsequently transferred to nitrocellulose membranes. Membranes were blocked with 5 % non-fat dry milk in Tris-buffered saline containing 0.05 % Tween-20 (TBST; 10 mM Tris-HCl, pH 7.5, 150 mM NaCl) for one hour at room temperature. Primary antibody incubations were performed overnight at 4 °C using the following antibodies: mouse anti-mTOR (1:1000; Abgent Biotechnology, San Diego, CA, USA) and mouse anti-β-actin (1:3000; Abgent Biotechnology). Following three TBST washes, membranes were incubated with horseradish peroxidase-conjugated goat anti-mouse IgG secondary antibody (1:50; KPL Biotechnology, Gaithersburg, MD, USA) for one hour at room temperature. Protein bands were visualized using an enhanced chemiluminescence (ECL) detection system (Pierce Biotechnology, Rockford, IL, USA). Densitometric analysis was performed using QuantiScan software, with β-actin serving as the loading control. All Western blot experiments were repeated at least three times using independent protein preparations.

Spinal cord injury model and cell transplantation

All animal procedures were approved by the Animal Research Committee of China Medical University and conducted in accordance with institutional guidelines for the care and use of laboratory animals. Sixty adult male Sprague-Dawley rats (230-250 g body weight) were obtained from the Chinese Medical University Laboratory Animal Center (Shenyang, China). Animals were housed under standard conditions with a 12-hour light/dark cycle and ad libitum access to food and water. A one-week acclimation period preceded all experimental procedures.

Rats were randomly assigned to three experimental groups (n=20 per group) using a computer-generated random-number sequence: (i) spinal cord injury with saline vehicle (SCI control group), (ii) SCI followed by transplantation of empty vector-transduced BMSCs (empty vector group), and (iii) SCI followed by transplantation of anti-miR-199a-3p-BMSCs (anti-miR-199a-3p group). Group allocation was performed by an investigator not involved in surgical procedures or behavioral scoring, with allocation concealed in sequentially numbered, opaque envelopes that were opened immediately prior to cell injection. Surgeons were aware of group assignment because of the identical appearance of cell suspensions across groups, but all behavioral assessments were conducted by two independent observers blinded to group assignment (see Section 2.9). Group size was selected a priori with reference to animal numbers used in comparable BMSC-transplantation studies employing rat contusion SCI models and longitudinal BBB locomotor assessment, in which approximately 12-20 animals were included per experimental group [15,16]. A formal a priori power calculation was not performed, and no *post hoc* power analysis was conducted. Exclusion criteria were defined prospectively as (i) failure to develop complete bilateral hindlimb paralysis immediately after contusion, (ii) intraoperative or perioperative death, or (iii) development of a severe urinary tract infection or persistent autophagia requiring humane euthanasia.

For surgical procedures, rats were anesthetized with intraperitoneal injection of sodium pentobarbital (50 mg/kg body weight) and positioned prone on a stereotaxic frame. A dorsal laminectomy was performed to expose the T10-T11 spinal cord segment. Contusion injury was induced using a standardized weight-drop method, in which a 20-g weight was released from a height of 10 cm onto the exposed spinal cord surface. Successful injury induction was confirmed by observation of hind limb retraction and tail flicking reflexes. Within 30 min following injury, rats received either saline (10 μl) or cell suspensions (10 μl containing approximately 1×10^5 cells) injected directly into the contusion epicenter using a Hamilton microsyringe. Injections were performed at a rate of 1 μl/min, and the needle was left in place for an additional 2 min following injection to minimize reflux. Postoperatively, all animals received intraperitoneal injections of buprenorphine at a dose of 20 μg/100 g body weight (0.2 mg/kg), administered four times at 3-hour intervals. Manual bladder expression was performed twice daily until spontaneous voiding returned, and prophylactic antibiotics (gentamicin, 5 mg/kg) were administered for the first three postoperative days to prevent urinary tract infections.

Behavioral assessment

Hindlimb locomotor function was evaluated at 1, 4, 7, 14, 21, 28, 35, and 42 days post-injury using the Basso-Beattie-Bresnahan (BBB) locomotor rating scale, a 21-point scale that systematically assesses hindlimb movement, weight support, coordination, and gait characteristics. Two investigators who were blinded to the experimental group assignments independently observed each animal in an open field for 4 min and scored locomotor function according to the established BBB criteria. The final score for each animal at each time point was calculated as the mean of the two observers' scores. Inter-rater reliability was assessed, and any discrepancies greater than two points were resolved through consensus evaluation.

Statistical analysis

All quantitative data are presented as mean ± standard deviation (SD). Statistical analyses were performed using SPSS version 17.0 software (SPSS Inc., Chicago, IL, USA). Comparisons among the three experimental groups were conducted using one-way analysis of variance (ANOVA) for normally distributed data, followed by Tukey's *post hoc* test for multiple pairwise comparisons. For BBB score analysis over time, two-way repeated measures ANOVA was employed to assess the effects of treatment group and time, as well as their interaction. Differences were considered statistically significant at $p<0.05$. All experiments were performed with a minimum of three independent biological replicates unless otherwise specified.

Results

Identification of differentially expressed microRNAs in BMSCs compared with neural cell populations

To elucidate the miRNA expression landscape that distinguishes BMSCs from cells of neural lineage, we performed comprehensive microarray profiling of BMSCs, cortical neurons, and neural stem cells. This comparative analysis revealed a distinct miRNA signature in BMSCs, with several miRNAs exhibiting marked differential expression relative to the neural cell populations (Table 1). Among the differentially expressed candidates, rno-miR-199a-3p emerged as the most prominently upregulated miRNA in BMSCs, with a mean normalized expression value of 2,730.96 in BMSCs compared with 0.70 in cortical neurons (approximately 3,910-fold higher) and 1.63 in neural stem cells (approximately 1,676-fold higher). To validate the microarray findings, we performed quantitative real-time RT-PCR analysis, which confirmed that miR-199a-3p expression was significantly elevated in BMSCs relative to miR-145, miR-143, and miR-214, the other differentially expressed miRNAs identified in the screen (Fig. 1A). These observations suggested that miR-199a-3p may serve as a molecular barrier to neuronal differentiation in BMSCs and thus warranted further functional investigation.

Construction and validation of the miR-199a-3p-sponge lentiviral expression system

To enable stable and sustained inhibition of miR-199a-3p function in BMSCs, we designed and constructed a lentiviral vector expressing a miR-199a-3p-sponge sequence. The sponge construct was engineered to contain multiple tandem miR-199a-3p binding sites with a central bulge region, which permits competitive sequestration of endogenous miR-199a-3p while evading miRNA-directed transcript degradation. Successful cloning of the rno-miR-199a-3p-sponge cassette into the pLVX-EGFP-IRES-neo backbone was confirmed through restriction enzyme digestion analysis. Double digestion

with XhoI and BamHI yielded the expected fragments, with an approximately 1.0-kb band corresponding to the EGFP-rno-miR-199a-3p-sponge insert and an approximately 8.0-kb band representing the vector backbone, as visualized by DNA agarose gel electrophoresis (Fig. 1B). Sanger sequencing further verified that the inserted sequence exhibited complete concordance with the designed target sequence, confirming the integrity of the construct.

Table 1. Differential miRNA expression profile in rat BMSCs compared with neural cell populations.

	BMSCs	Cortical neurons	Neural stem cells
rno-miR-199a-3p_st	2730.96	0.6982638	1.628999
rno-miR-145_st	1357.96	1.559705	2.357869
rno-miR-143_st	1253.63	0.8669992	1.947834
rno-miR-214_st	1299.59	1.010691	0.9664773
rno-miR-199a-5p_st	639.96	0.7110068	0
rno-miR-152_st	951.2946	2.670309	23.96128
rno-miR-196a_st	185.6279	0.7502214	0.8354928

GeneChip microarray analysis was performed on total RNA isolated from BMSCs, cortical neurons, and neural stem cells. The table presents miRNAs exhibiting significant upregulation in BMSCs relative to both neural cell types. Differential expression was defined as fold change >2.0 with adjusted $p<0.05$. Values represent mean fold change from three independent biological replicates.

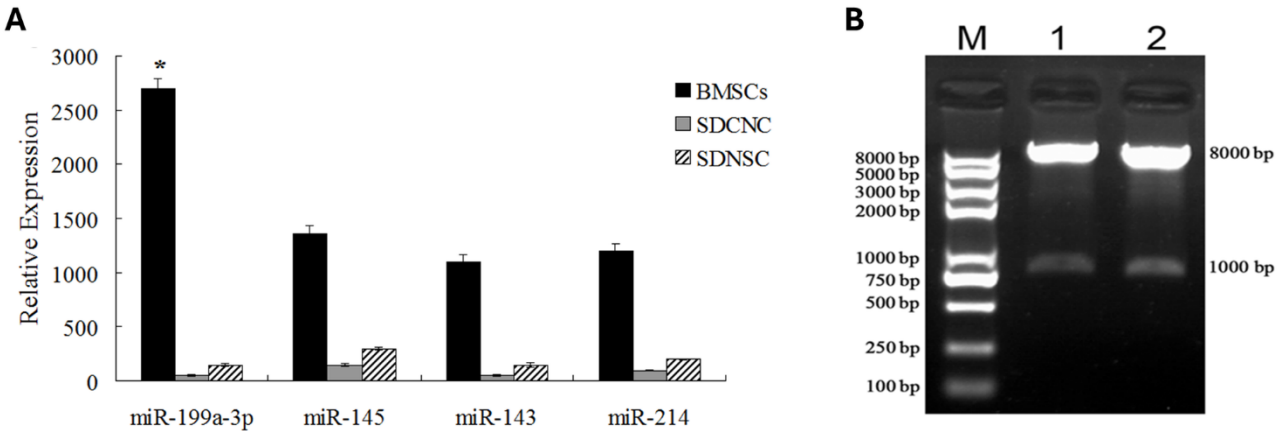


Fig. 1. Identification of differentially expressed miRNAs and construction of the miR-199a-3p-sponge lentiviral vector. (**A**) Quantitative RT-PCR analysis of miRNA expression in BMSCs. Among the differentially expressed miRNAs identified by microarray analysis, miR-199a-3p exhibited the most pronounced upregulation in BMSCs compared with miR-145, miR-143, and miR-214. Expression levels were normalized to U6 small nuclear RNA. Data are presented as mean ± SEM. $p<0.05$ vs. other miRNAs; one-way ANOVA with Tukey's *post hoc* test; n=3 independent experiments. (**B**) Verification of pLVX-EN-rno-miR-199a-3p-sponge vector construction by restriction enzyme digestion. The plasmid was digested with XhoI and BamHI and analyzed by agarose gel electrophoresis. Lane M: DNA Marker III; Lane 1: Undigested pLVX-199a-3p-sponge plasmid; Lane 2: Digested plasmid showing the expected fragments, including an approximately 1.0-kb band corresponding to the EGFP-rno-miR-199a-3p-sponge insert and an approximately 8.0-kb band corresponding to the vector backbone.

Efficient lentiviral production and transduction of BMSCs

Following transfection of 293FT packaging cells with the lentiviral vector system, viral production efficiency was assessed through serial dilution analysis. At the initial (1E-0) dilution, abundant GFP-positive cells were readily observed (Fig. 2B), demonstrating robust viral production. Progressive dilution resulted in a corresponding decrease in GFP-positive cells, with the sixth dilution (1E-6) yielding two detectable GFP-positive cells (Fig. 2N). Based on this limiting dilution analysis, the viral titer was calculated to be 1.0×10^9 TU/ml, which was deemed suitable for subsequent transduction experiments.

Transduction of BMSCs with either the pLVX-EN-rno-miR-199a-3p-sponge (anti-miR-199a-3p group) or the empty control vector pLVX-EN-rno (empty vector

group) resulted in efficient gene delivery, as evidenced by widespread GFP expression. Quantitative RT-PCR analysis revealed that BMSCs transduced with the miR-199a-3p-sponge construct exhibited a marked reduction in miR-199a-3p expression, compared with untransduced control BMSCs and compared with empty vector-transduced BMSCs (Fig. 2O). This reduction was statistically significant ($p<0.01$), confirming effective functional inhibition of miR-199a-3p by the sponge construct.

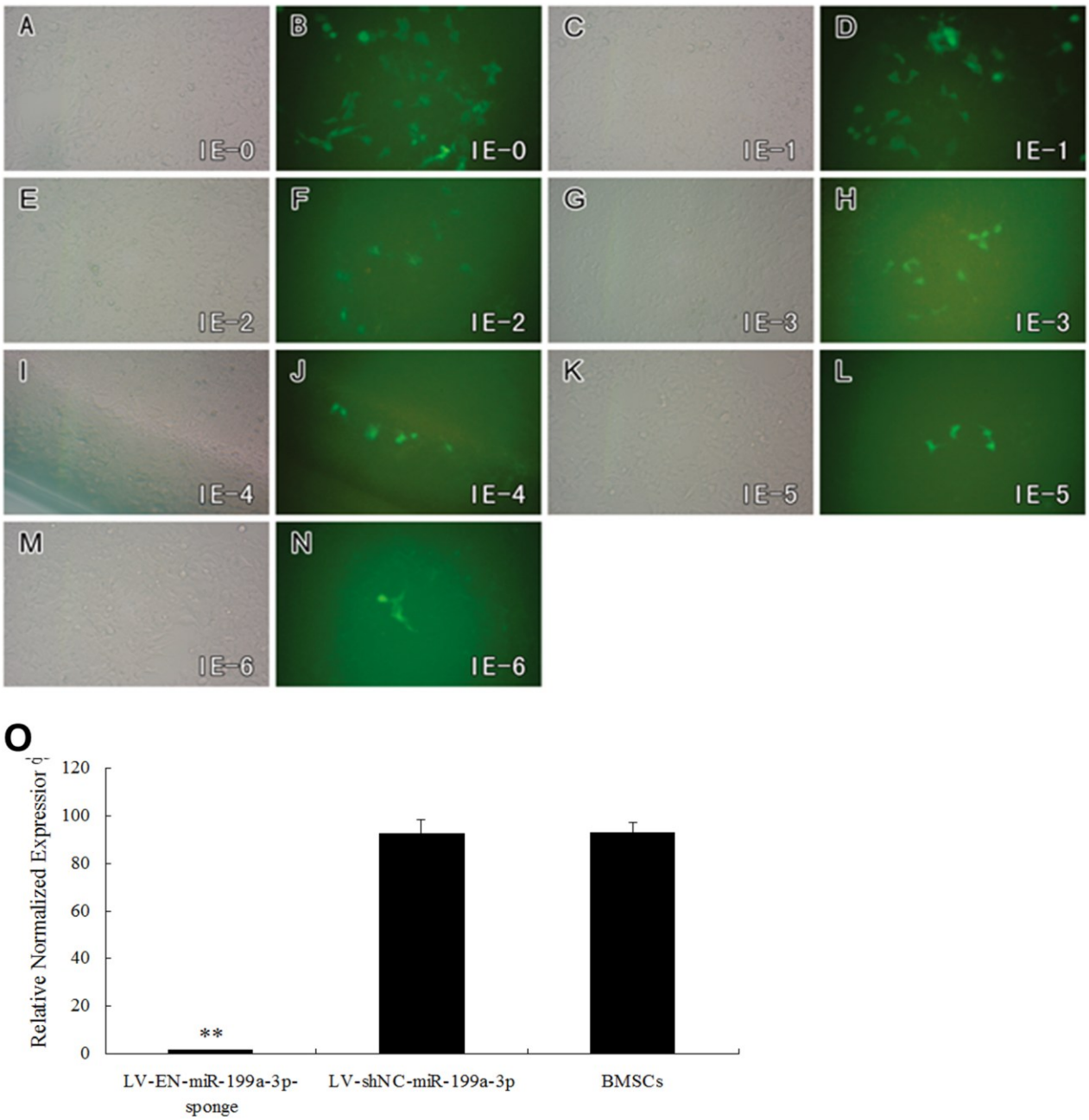


Fig. 2. Lentiviral titer determination and validation of miR-199a-3p knockdown efficiency. (**A-N**) Determination of lentiviral titer by serial dilution. 293FT packaging cells were transduced with the pLVX-EN-rno-miR-199a-3p-sponge lentivirus, and viral titer was assessed by quantification of GFP-positive cells across serial dilutions. Representative fluorescence microscopy images are shown for each dilution. (**A, B**) At the initial dilution (1E-0), abundant GFP-positive cells were observed. (**C-L**) Progressive dilutions (1E-1 through 1E-5) showing decreasing numbers of GFP-positive cells. (**M, N**) At the 1E-6 dilution, two GFP-positive cells were detected, yielding a calculated viral titer of 1.0×10^9 TU/ml. (**O**) Quantitative RT-PCR analysis confirming reduced miR-199a-3p expression following sponge transduction. BMSCs were transduced with pLVX-EN-rno-miR-199a-3p-sponge (anti-miR-199a-3p group), the empty vector pLVX-EN-rno (empty vector group), or left untransduced (control group). miR-199a-3p expression was normalized to U6. Data are presented as mean ± SEM. ** $p<0.01$ vs. control and empty vector groups; one-way ANOVA with Tukey's *post hoc* test; n=3 independent experiments.

Downregulation of miR-199a-3p elevates mTOR protein expression

Given that mTOR has been previously identified as a direct target of miR-199a-3p, we examined whether sponge-mediated inhibition of miR-199a-3p would result in derepression of mTOR protein expression. Western blot analysis was performed on lysates from all three experimental groups following six days of *in vitro* culture. The results demonstrated that mTOR protein levels were elevated in the anti-miR-199a-3p group compared with both the control and empty vector groups (Fig. 3A). Densitometric quantification, normalized to β-actin and expressed in relative optical-density units, confirmed that mTOR expression was increased compared with control and compared with the empty vector group, and that these increases were statistically significant ($p<0.01$; Fig. 3B). The inverse relationship between miR-199a-3p levels and mTOR protein expression provided functional validation of effective miR-199a-3p inhibition and confirmed the regulatory relationship between this miRNA and its target in the BMSC model system.

Anti-miR-199a-3p BMSCs acquire neuronal markers and neurite-like morphology in vitro

To investigate the neurogenic potential of miR-199a-3p-inhibited BMSCs, we performed immunofluorescence analysis of established neuronal markers in anti-miR-199a-3p BMSCs after six days of *in vitro* culture under standard growth conditions (no exogenous neurogenic supplements were added; see Section 2.5). β-III tubulin, a cytoskeletal protein characteristic of immature neurons, and MAP-2, a dendritic marker associated with mature neuronal phenotypes, were selected as indicators of acquisition of a neuronal-like phenotype.

Anti-miR-199a-3p BMSCs displayed robust immunoreactivity for both β-III tubulin (Fig. 4A, green fluorescence) and MAP-2 (Fig. 4B, red fluorescence). Both markers were detected throughout the cell soma and along elongated neurite-like processes. The matched phase-contrast images (Fig. 4A2, A4, B2, B4) show that anti-miR-199a-3p BMSCs adopted a morphology characterized by extended dendrite-like and neurite-like projections, consistent with acquisition of a neuronal-like phenotype. Matched immunofluorescence images were not captured for the control and empty vector groups; therefore, between-group quantitative comparison in this study is provided by the mTOR Western blot (Fig. 3), which shows significant derepression of mTOR in the anti-miR-199a-3p group relative to both the control and empty vector groups. This derepression is a validated molecular readout of effective miR-199a-3p inhibition. The comparison is further supported by the significantly improved *in vivo* functional recovery in transplanted animals (Fig. 5, described in Section 3.6).

Because the neuronal identity of these cells was assessed on the basis of marker expression and morphology only, we refer to this response as "neuronal-like differentiation" and note that functional demonstration of mature neuronal properties (e.g., electrophysiology, synaptic connectivity) is beyond the scope of the present study.

Transplantation of anti-miR-199a-3p-BMSCs promotes functional recovery following spinal cord injury

To evaluate the therapeutic potential of miR-199a-3p-inhibited BMSCs *in vivo*, we employed a rat contusion spinal cord injury model. Immediately following injury, all animals exhibited complete bilateral hindlimb paralysis, confirming successful injury induction. Locomotor function was subsequently monitored over a 42-day recovery period using the BBB rating scale.

Spontaneous functional recovery was observed in all three experimental groups over the evaluation period, as reflected by gradual increases in BBB scores. However, the trajectory and extent of recovery differed substantially among groups. Beginning at day 14 post-injury, animals receiving anti-miR-199a-3p-BMSC transplants demonstrated significantly greater hindlimb locomotor recovery compared with both the SCI control group and the empty vector group (day 14, $p<0.05$; days 21 and 28, $p<0.01$; Fig. 5).

This differential recovery was sustained throughout the observation period. At the terminal time point of six weeks post-injury, mean BBB scores were 10.8±0.6 in the SCI control group, 13.0±0.8 in the empty vector group, and 15.7±0.6 in the anti-miR-199a-3p group (Fig. 5), corresponding to differences of 4.9 points (anti-miR-199a-3p vs. SCI control) and 2.7 points (anti-miR-199a-3p vs. empty vector) on the 21-point BBB scale. Statistical analysis confirmed that the anti-miR-199a-3p group achieved significantly superior functional outcomes compared with both comparison groups ($p<0.05$). These *in vivo* findings demonstrate that inhibition of miR-199a-3p in BMSCs enhances their capacity to promote functional recovery when transplanted into the injured spinal cord, supporting the therapeutic relevance of this molecular intervention strategy.

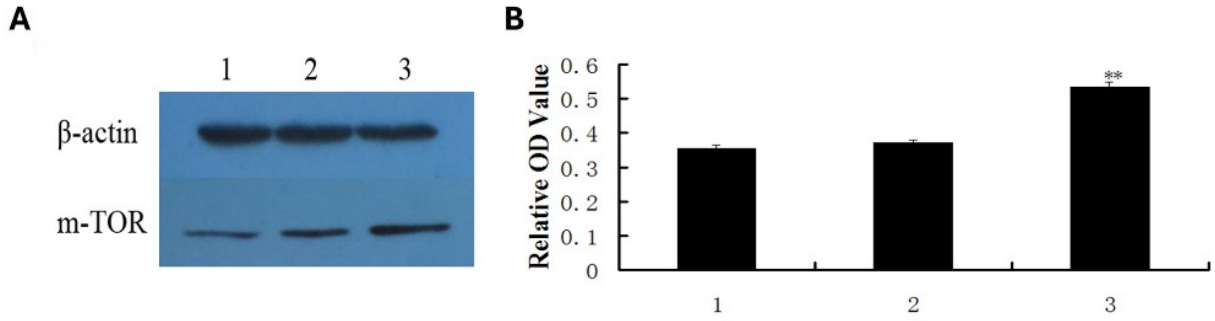


Fig. 3. Inhibition of miR-199a-3p increases mTOR protein expression in BMSCs. (**A**) Representative Western blot analysis of mTOR protein expression following six days of in vitro culture. Lane 1: Control group (untransduced BMSCs); Lane 2: Empty vector group (empty vector-transduced BMSCs); Lane 3: Anti-miR-199a-3p group (miR-199a-3p-sponge-transduced BMSCs). β-actin served as the loading control. (**B**) Densitometric quantification of mTOR protein levels normalized to β-actin. Data are presented as mean ± SEM in relative optical-density units. ** $p<0.01$ vs. control and empty vector groups; one-way ANOVA with Tukey's *post hoc* test; n=3 independent experiments.

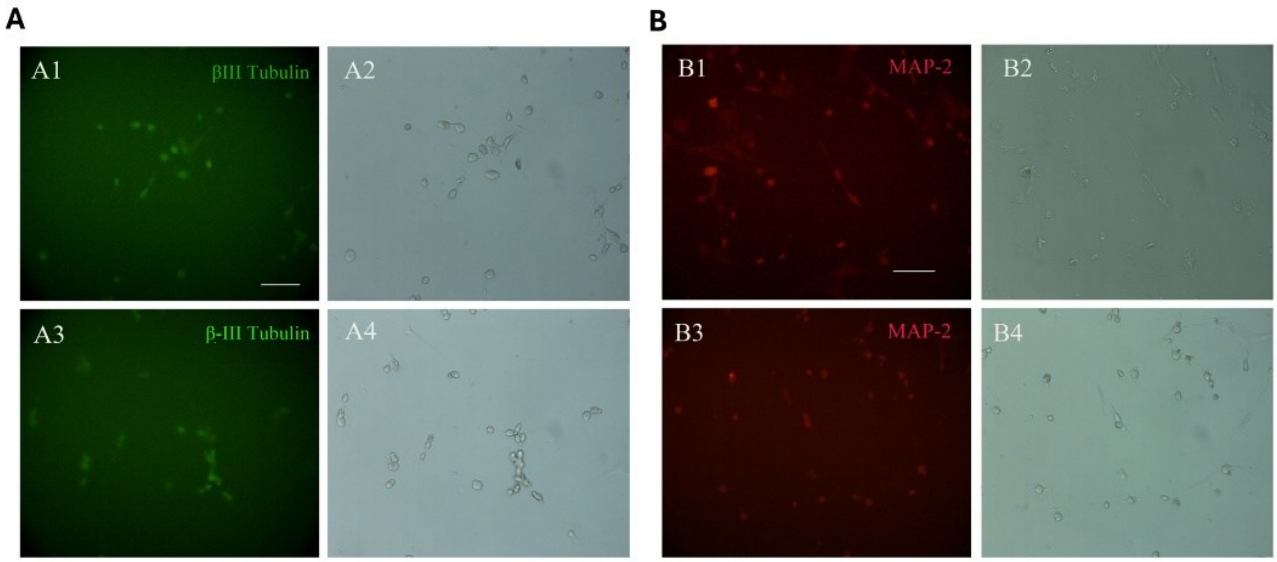


Fig. 4. Neuronal marker expression and neurite-like morphology in anti-miR-199a-3p BMSCs. Representative immunofluorescence and matched phase-contrast images of BMSCs transduced with pLVX-EN-rno-miR-199a-3p-sponge (anti-miR-199a-3p group) after six days of in vitro culture. (**A**) β-III tubulin immunostaining (green fluorescence) in two representative fields (A1 and A3), with matched phase-contrast images of the same fields (A2 and A4). (**B**) MAP-2 immunostaining (red fluorescence) in two representative fields (B1 and B3), with matched phase-contrast images of the same fields (B2 and B4). Both β-III tubulin and MAP-2 were detected in cell soma and along neurite-like processes; anti-miR-199a-3p BMSCs displayed extended dendrite-like and neurite-like projections consistent with acquisition of a neuronal-like phenotype. Matched immunofluorescence images of the control and empty vector groups were not acquired in this experiment; the corresponding between-group comparison is provided by the mTOR Western blot in Figure 3 and the *in vivo* functional recovery data in Figure 5. Scale bars = 100 μm. Magnification: 200×. Images are representative of three independent experiments.

Discussion

In this study, we identified miR-199a-3p as a key regulator of neuronal-like differentiation in rat BMSCs. Through comparative miRNA profiling of BMSCs, cortical neurons, and neural stem cells, we found that miR-199a-3p was substantially upregulated in BMSCs relative to neural cell populations, a finding confirmed by qRT-PCR analysis. Functional studies demonstrated that inhibition of miR-199a-3p using a lentiviral sponge construct enhanced neuronal marker expression and neurite-like morphology *in vitro* and promoted functional recovery following spinal cord injury *in vivo*. These findings suggest that miR-199a-3p acts as a molecular constraint on the neurogenic potential of BMSCs and that its targeted inhibition may represent a viable strategy for enhancing BMSC-based therapies for neural repair.

The miRNA miR-199a-3p has been previously characterized in the context of cancer biology, where it is

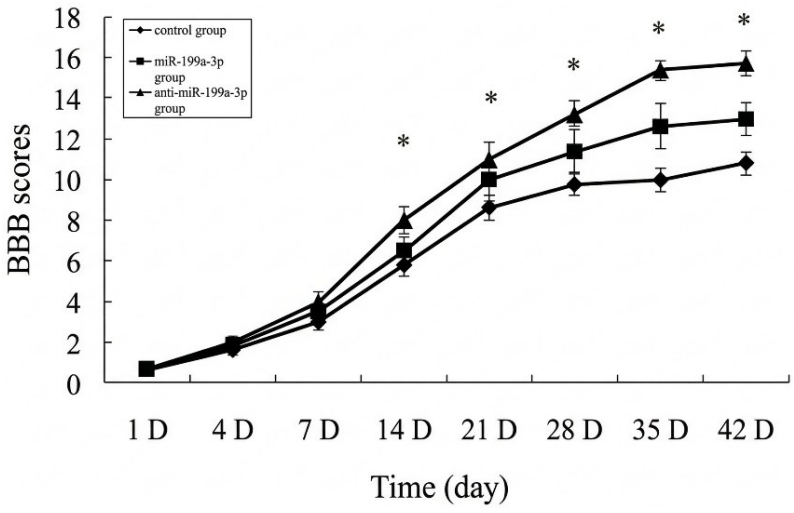


Fig. 5. Transplantation of anti-miR-199a-3p-BMSCs improves functional recovery following spinal cord injury. Hindlimb locomotor function was assessed using the Basso-Beattie-Bresnahan (BBB) rating scale from day 1 through day 42 following contusion spinal cord injury at the T10-T11 level. Rats received transplantation of saline vehicle (SCI control group, n=20), empty vector-transduced BMSCs (empty vector group, n=20), or miR-199a-3p-sponge-transduced BMSCs (anti-miR-199a-3p group, n=20) within 30 min of injury. The anti-miR-199a-3p group demonstrated significantly greater locomotor recovery compared with both the SCI control group and the empty vector group beginning at day 14 post-injury. Data are presented as mean ± SD. * $p<0.05$; two-way repeated-measures ANOVA with Tukey's *post hoc* test was used to assess group differences across time points.

frequently downregulated in hepatocellular carcinoma [17], bladder cancer [18], ovarian cancer [19], and osteosarcoma [20]. These observations have led to its classification as a potential tumor suppressor, with reduced expression associated with enhanced cellular proliferation and transformation. Our finding that miR-199a-3p is highly expressed in BMSCs and that its inhibition promotes acquisition of neuronal markers adds a new dimension to the functional repertoire of this miRNA, suggesting context-dependent roles that extend beyond oncogenic regulation.

The mechanistic basis for miR-199a-3p regulation of neuronal-like differentiation likely involves its targeting of mTOR. Previous work has established that miR-199a-3p binds directly to the 3′-UTR of mTOR mRNA, resulting in translational repression [21,22]. Consistent with this regulatory relationship, we observed that sponge-mediated inhibition of miR-199a-3p in BMSCs led to a significant increase in mTOR protein expression. The mTOR kinase functions as a central regulator of cap-dependent protein translation and plays a critical role in cellular growth and metabolism [23,24]. In the nervous system, mTOR signaling has been shown to promote axonal elongation and regeneration [25]. Notably, genetic activation of the mTOR pathway through conditional deletion of PTEN, a negative regulator of mTOR signaling, promotes robust axonal regeneration in the injured central nervous system [25,26]. Since neuronal growth and differentiation require substantial new protein synthesis to provide the building blocks for axonal extension and synapse formation, enhanced mTOR activity would be expected to support these processes [27].

Our *in vitro* findings demonstrated that anti-miR-199a-3p BMSCs expressed both β-III tubulin, a marker of immature neurons, and MAP-2, a dendritic protein associated with mature neuronal phenotypes, and adopted extended dendrite-like and neurite-like processes, which are morphological features consistent with acquisition of a neuronal-like phenotype. The primary between-group quantitative readouts supporting a functional consequence of miR-199a-3p inhibition are the derepression of mTOR by Western blot in the anti-miR-199a-3p group relative to control and empty vector groups and the significantly improved locomotor recovery of transplanted animals; the immunofluorescence images in Figure 4 characterize the neuronal-like phenotype of anti-miR-199a-3p BMSCs but were not acquired for the control and empty vector groups under matched conditions. Taken together, these observations indicate that relieving miR-199a-3p-mediated suppression of mTOR is sufficient to promote neurogenic changes in BMSCs, at least under the culture conditions employed in this study. We deliberately use the qualifier "neuronal-like" throughout because β-III tubulin and MAP-2 immunoreactivity together with neurite-like morphology, while consistent with commitment along a neuronal lineage, do not on their own establish mature neuronal identity in the absence of electrophysiological or synaptic evidence.

The therapeutic relevance of these findings was supported by our *in vivo* experiments. Transplantation of anti-miR-199a-3p-BMSCs into rats following contusion spinal cord injury resulted in significantly improved locomotor recovery compared with both SCI control and empty vector-transplanted animals. Enhanced functional

outcomes were evident from day 14 post-injury onward.

Several mechanisms could underlie the observed functional improvement, and it is important to acknowledge that recovery is unlikely to reflect neuronal replacement by transplanted cells alone. First, direct neural repair may be achieved through enhanced neuronal-like differentiation of transplanted BMSCs, contributing to circuit reconstruction and axonal bridging. Second, paracrine effects of transplanted BMSCs are increasingly recognized as a dominant mechanism of BMSC-mediated neural repair. BMSCs secrete a broad panel of neurotrophic factors (including BDNF, NGF, GDNF, and VEGF), growth-promoting cytokines, and extracellular vesicles that can support neuronal survival, promote endogenous axonal regeneration, stimulate angiogenesis, and modulate the extracellular matrix at the injury site [28,29]. Because mTOR activity is closely linked to secretome composition and cellular biosynthetic capacity, miR-199a-3p inhibition may plausibly enhance not only intrinsic neurogenic potential but also the paracrine repertoire of the transplanted cells; direct measurement of secretome composition was not performed in the present study and represents a productive direction for future work. Third, BMSCs are well documented to exert immunomodulatory effects at sites of central nervous system injury, including polarization of microglia and infiltrating macrophages toward pro-regenerative phenotypes, attenuation of pro-inflammatory cytokine release, and reduction of secondary tissue damage [28,29]. Fourth, improved survival or engraftment of miR-199a-3p-inhibited cells in the hostile post-injury microenvironment, potentially because of enhanced mTOR-driven biosynthetic and stress-adaptive capacity, could increase the effective duration of these paracrine and immunomodulatory effects. The relative contribution of each of these mechanisms was not directly dissected in the present study, and disentangling neural replacement from paracrine and immunomodulatory effects will require additional experiments including cell fate tracking, conditioned medium/exosome studies, and immune-cell profiling of the injury site.

The miRNA sponge approach employed in this study offers certain advantages for sustained miRNA inhibition. Sponge constructs contain multiple tandem binding sites complementary to the target miRNA but incorporate a central bulge region that prevents Argonaute-mediated cleavage of the sponge transcript [30]. This design enables competitive sequestration of the endogenous miRNA, effectively reducing its availability to suppress natural mRNA targets. Lentiviral delivery of the sponge sequence permits stable integration and long-term expression, making this approach suitable for cell-based therapeutic applications where sustained modification is desirable. Recent studies published in Physiological Research have likewise demonstrated that miRNA modulation can attenuate neural injury and that mesenchymal stromal cells can exert tissue-protective and immunomodulatory effects, supporting the broader relevance of miRNA-directed and MSC-based regenerative strategies [31,32].

Limitations

Several limitations of this study should be acknowledged. First, neuronal identity of miR-199a-3p-inhibited BMSCs *in vitro* was inferred from expression of β-III tubulin and MAP-2 together with neurite-like morphology; we did not perform electrophysiological recordings, calcium imaging, or synaptic connectivity assays to confirm that these cells acquire functional neuronal properties, and we therefore refer to the observed response as neuronal-like differentiation rather than mature neurogenesis. Second, we did not perform direct *in vivo* lineage tracing or fate mapping of transplanted BMSCs, and consequently the survival, engraftment, migration, and terminal differentiation of anti-miR-199a-3p-BMSCs within the injured spinal cord were not directly assessed; the observed improvement in BBB scores therefore cannot be unambiguously attributed to neuronal replacement by the transplanted cells and, as discussed above, is likely to reflect a combination of neural, paracrine, and immunomodulatory effects. Third, although mTOR represents a well-characterized target of miR-199a-3p and its derepression is consistent with the observed phenotypes, miRNAs canonically regulate hundreds of targets; miR-199a-3p likely regulates additional messenger RNAs relevant to stem-cell biology, cytoskeletal dynamics, and neural fate that may contribute to the observed effects, and rescue experiments (e.g., mTOR inhibition in anti-miR-199a-3p BMSCs) were not performed to formally establish the necessity of mTOR in this system. Fourth, the study relies on a single rat model (contusion SCI at T10-T11), a single cell source (Cyagen-supplied SD rat BMSCs, passages 3-5), and a single time window of behavioral follow-up (42 days); generalizability to other injury models, chronic time points, species (including human BMSCs), and

clinical translation therefore remains to be established. Fifth, matched immunofluorescence images of the control and empty vector groups were not acquired under the same conditions as those of the anti-miR-199a-3p group; the between-group quantitative comparison in this study is therefore anchored on the mTOR Western blot and the *in vivo* BBB recovery data, and the immunofluorescence images in Figure 4 should be interpreted as characterizing the neuronal-like phenotype of anti-miR-199a-3p BMSCs rather than as a direct visual quantitative comparison across the three groups. Sixth, sample size (n=20 per group *in vivo*, n=3 biological replicates *in vitro*) was selected on the basis of comparable published SCI transplantation studies rather than a formal a priori power calculation, and no post-hoc power analysis was performed because such analyses are not statistically informative once results are known; effect sizes and their confidence intervals should therefore be interpreted with the reported group sizes in mind. Future studies employing single-cell transcriptomic analysis, electrophysiological characterization of derived cells, *in vivo* lineage tracing (e.g., GFP+ or luciferase-based tracking), rescue experiments targeting mTOR, secretome and immune-profiling assays, and validation across additional models and human-derived BMSCs will provide deeper mechanistic insight and strengthen the translational relevance of this strategy.

Conclusions

In summary, our study identifies miR-199a-3p as a negative regulator of neuronal-like differentiation in rat BMSCs. Inhibition of miR-199a-3p enhances neurogenic marker expression *in vitro* through a mechanism involving derepression of mTOR and promotes functional recovery following spinal cord injury *in vivo*. These findings provide a foundation for further development of miRNA-based strategies to enhance the therapeutic efficacy of BMSC transplantation for spinal cord injury and potentially other neurological conditions.

Conflict of Interest

There is no conflict of interest.

Acknowledgements

This work was supported by the Liaoning Province Joint Fund General Program (Grant Nos. 2023-MSLH-128 and 2023-MSLH-122).

References

1. Hu X, Xu W, Ren Y, Wang Z, He X, Huang R, et al. Spinal cord injury: molecular mechanisms and therapeutic interventions. Signal Transduct Target Ther 2023;8:245. https://doi.org/10.1038/s41392-023-01477-6
2. Zeng CW. Stem cell-based approaches for spinal cord injury: the promise of iPSCs. Biology (Basel) 2025;14:314. https://doi.org/10.3390/biology14030314
3. Ramos-Zúñiga R, González-Pérez O, Macías-Ornelas A, Capilla-Gonzalez V, Quiñones-Hinojosa A. Ethical implications in the use of embryonic and adult neural stem cells. Stem Cells Int 2012;2012:470949. https://doi.org/10.1155/2012/470949
4. Zhidu S, Ying T, Rui J, Chao Z. Translational potential of mesenchymal stem cells in regenerative therapies for human diseases: challenges and opportunities. Stem Cell Res Ther 2024;15:266. https://doi.org/10.1186/s13287-024-03885-z
5. Purwaningrum M, Jamilah NS, Purbantoro SD, Sawangmake C, Nantavisai S. Comparative characteristic study from bone marrow-derived mesenchymal stem cells. J Vet Sci 2021;22:e74. https://doi.org/10.4142/jvs.2021.22.e74
6. Xu Q, Hou W, Zhao B, Fan P, Wang S, Wang L, Gao J. Mesenchymal stem cells lineage and their role in disease development. Mol Med 2024;30:207. https://doi.org/10.1186/s10020-024-00967-9
7. Han X, Liao R, Li X, Zhang C, Huo S, Qin L, et al. Mesenchymal stem cells in treating human diseases: molecular mechanisms and clinical studies. Signal Transduct Target Ther 2025;10:262. https://doi.org/10.1038/s41392-025-02313-9
8. Ergin K, Çetinkaya R. Regulation of microRNAs. Methods Mol Biol 2022;2257:1-32. https://doi.org/10.1007/978-1-0716-1170-8_1
9. Ghosh S, Kumar V, Mukherjee H, Lahiri D, Roy P. Nutraceutical regulation of miRNAs involved in neurodegenerative diseases and brain cancers. Heliyon 2021;7:e07262. https://doi.org/10.1016/j.heliyon.2021.e07262

10. Victor MB, Richner M, Hermanstyne TO, Ransdell JL, Sobieski C, Deng PY, et al. Generation of human striatal neurons by microRNA-dependent direct conversion of fibroblasts. Neuron 2014;84:311-323. https://doi.org/10.1016/j.neuron.2014.10.016
11. Gu X, Weng R, Hou J, Liu S. Endothelial miR-199a-3p regulating cell adhesion molecules by targeting mTOR signaling during inflammation. Eur J Pharmacol 2022;925:174984. https://doi.org/10.1016/j.ejphar.2022.174984
12. Liu X, Wang X, Chai B, Wu Z, Gu Z, Zou H, et al. miR-199a-3p/5p regulate tumorgenesis via targeting Rheb in non-small cell lung cancer. Int J Biol Sci 2022;18:4187-4202. https://doi.org/10.7150/ijbs.70312
13. Zhang J, Gan W, Peng R, Lu L, Lu W, Liu J. Activation of the mTOR pathway promotes neurite growth through upregulation of CD44 expression. J Int Med Res 2023;51:3000605231178510. https://doi.org/10.1177/03000605231178510
14. Al-Ali H, Ding Y, Slepak T, Wu W, Sun Y, Martinez Y, et al. The mTOR substrate S6 kinase 1 (S6K1) is a negative regulator of axon regeneration and a potential drug target for central nervous system injury. J Neurosci 2017;37:7079-7095. https://doi.org/10.1523/JNEUROSCI.0931-17.2017
15. Li F, Fei D, Sun L, Zhang S, Yuan Y, Zhang L, et al. Neuroprotective effect of bone marrow stromal cell combination with atorvastatin in rat model of spinal cord injury. Int J Clin Exp Med 2014;7:4967-4974.
16. Kang ES, Ha KY, Kim YH. Fate of transplanted bone marrow derived mesenchymal stem cells following spinal cord injury in rats by transplantation routes. J Korean Med Sci 2012;27:586-593. https://doi.org/10.3346/jkms.2012.27.6.586
17. Liu AG, Pang YY, Chen G, Wu HY, He RQ, Dang YW, et al. Downregulation of miR-199a-3p in hepatocellular carcinoma and its relevant molecular mechanism via GEO, TCGA database and in silico analyses. Technol Cancer Res Treat 2020;19:1533033820979670. https://doi.org/10.1177/1533033820979670
18. Sakaguchi T, Yoshino H, Yonemori M, Miyamoto K, Sugita S, Matsushita R, et al. Regulation of ITGA3 by the dual-stranded microRNA-199 family as a potential prognostic marker in bladder cancer. Br J Cancer 2017;116:1077-1087. https://doi.org/10.1038/bjc.2017.43
19. Cui Y, Wu F, Tian D, Wang T, Lu T, Huang X, et al. miR-199a-3p enhances cisplatin sensitivity of ovarian cancer cells by targeting ITGB8. Oncol Rep 2018;39:1649-1657. https://doi.org/10.3892/or.2018.6259
20. Duan Z, Choy E, Harmon D, Liu X, Susa M, Mankin H, et al. MicroRNA-199a-3p is downregulated in human osteosarcoma and regulates cell proliferation and migration. Mol Cancer Ther 2011;10:1337-1345. https://doi.org/10.1158/1535-7163.MCT-11-0096
21. Kar AN, Lee SJ, Sahoo PK, Thames E, Yoo S, Houle JD, Twiss JL. MicroRNAs 21 and 199a-3p regulate axon growth potential through modulation of Pten and mTor mRNAs. eNeuro 2021;8:ENEURO.0155-21.2021. https://doi.org/10.1523/ENEURO.0155-21.2021
22. Wu D, Huang HJ, He CN, Wang KY. MicroRNA-199a-3p regulates endometrial cancer cell proliferation by targeting mammalian target of rapamycin (mTOR). Int J Gynecol Cancer 2013;23:1191-1197. https://doi.org/10.1097/IGC.0b013e31829ea779
23. Panwar V, Singh A, Bhatt M, Tonk RK, Azizov S, Raza AS, et al. Multifaceted role of mTOR (mammalian target of rapamycin) signaling pathway in human health and disease. Signal Transduct Target Ther 2023;8:375. https://doi.org/10.1038/s41392-023-01608-z
24. Bodine SC. The role of mTORC1 in the regulation of skeletal muscle mass. Fac Rev 2022;11:32. https://doi.org/10.12703/r/11-32
25. Crino PB. Mechanistic target of rapamycin (mTOR) signaling in status epilepticus. Epilepsy Behav 2019;101:106550. https://doi.org/10.1016/j.yebeh.2019.106550
26. Shi Z, Mao L, Chen S, Du Z, Xiang J, Shi M, et al. Reversing persistent PTEN activation after traumatic brain injury fuels long-term axonal regeneration via Akt/mTORC1 signaling cascade. Adv Sci (Weinh) 2025;12:2410136. https://doi.org/10.1002/advs.202410136
27. Twiss JL, Buchanan CN. Regulation of subcellular protein synthesis for restoring neural connectivity. Int J Mol Sci 2025;26:7283. https://doi.org/10.3390/ijms26157283
28. Luo Z, Wu F, Xue E, Huang L, Yan P, Pan X, Zhou Y. Hypoxia preconditioning promotes bone marrow mesenchymal stem cells survival by inducing HIF-1α in injured neuronal cells derived exosomes culture system. Cell Death Dis 2019;10:134. https://doi.org/10.1038/s41419-019-1410-y

29. Pang QM, Qian NN, Zou WH, Yang YC, Chen H, Zhang M, et al. PBMSCs transplantation facilitates functional recovery after spinal cord injury by regulating microglia/macrophages plasticity. Transpl Immunol 2022;72:101592. https://doi.org/10.1016/j.trim.2022.101592
30. Diener C, Keller A, Meese E. The miRNA-target interactions: an underestimated intricacy. Nucleic Acids Res 2024;52:1544-1557. https://doi.org/10.1093/nar/gkad1142
31. Wang X, Li M, Hu Y. miR-29c-3p attenuates β-amyloid-induced neurotoxicity in Alzheimer's disease through regulating β-site amyloid precursor protein-cleaving enzyme 1. Physiol Res 2023;72:833-841. https://doi.org/10.33549/physiolres.935084
32. Chen Z, Ruan B, Long G, Lin W. Adipose tissue-derived mesenchymal stem cells attenuate lung inflammation and fibrosis in the bleomycin-induced pulmonary fibrosis rat model via caveolin-1/NF-κB signaling axis. Physiol Res 2022;71:657-666. https://doi.org/10.33549/physiolres.934892